ELECTRONIC SUPPORTING INFORMATION

A unique microporous copper-trimesate selenite with selective CO$_2$ sorption capability

Giannis. S. Papaefstathiou,[a] **Kota S. Subrahmanyam,**[b] **Gerasimos. S. Armatas,**[c] **Christos. D. Malliakas,**[b] **Mercouri. G. Kanatzidis** [b] **and Manolis. J. Manos** *[c]

[a] Chemistry Department, National and Kapodistrian University of Athens, 15771 Athens, Greece
[b] Chemistry Department, Northwestern University, Evanston, IL 60208, USA
[c] Department of Materials Science and Technology, University of Crete, 71003 Heraklion, Greece
[d] Chemistry Department, University of Ioannina, 45510 Ioannina, Greece
Email:emanos@cc.uoi.gr

EXPERIMENTAL SECTION

Materials. Reagent grade chemicals were obtained from Aldrich and used without further purification.

Syntheses.

MINOF-1: A solution of $Cu(NO_3)_2 \cdot 3H_2O$ (0.325 g, 1.35 mmol) in water (4 mL) was added into a stirred solution of H_3btc (0.140 g, 0.67 mmol) in ethanol (4 mL), in a Teflon cup. Stirring the mixture for ~ 5 min resulted in a formation of a blue precipitate. Then, solid KSeCN (0.194 g, 1.35 mmol) was added to the above suspension and almost immediately, a dark-brown solid was formed. The Teflon cup was transferred into a 23 mL Teflon-lined stainless steel autoclave. The autoclave was sealed and placed in an oven operated at 90 ˚C, remained undisturbed at this temperature for 20 h and then was allowed to cool at room temperature. A mixture of large turquoise plate-like crystals of **MINOF-1** and unidentified brown powder were isolated by filtration. The crystals of **MINOF-1** were separated from the powder by using a test sieve. Yield: 0.1 g. Compound **MINOF-1** was analyzed as **MINOF-1**$\cdot 6H_2O$. Anal. Calc. for $C_{18}H_{22}Cu_4O_{23}Se$: C, 23.01; H, 2.36; N, 0. Found: C, 23.12; H, 2.26; N, 0.

IR, thermal and elemental analyses. Infrared spectra (IR) in the mid-IR region [4000-400 cm^{-1}] were obtained in KBr pellets with a Perkin-Elmer Spectrum GX FT-IR spectrometer. The sample of **MINOF-1'** for the IR measurement was prepared by heating the KBR pellet of **MINOF-1** under vacuum at 150 ^{0}C for ~ 20 h. Thermogravimetric analysis (TGA) was carried out with a Shimatzu TGA 50. Samples (10±0.5 mg) were placed in quartz crucible. Samples were heated from ambient temperature to 500 ^{o}C in a 20 ml/min flow of N_2 or air. Heating rate of 10 ^{o}C/min was used and continuous records of sample temperature, sample weight and its first derivative (DTG) were taken. Elemental analyses (C, H, N) were performed by the in-house facilities of the University of Cyprus, Chemistry Department, Nicosia, Cyprus.

Scanning Electron Microscopy (SEM). Images of crystals were obtained using Hitachi S-3500 scanning electron microscope (SEM) with an accelerating voltage of 20 kV and working distance 10.6 mm. The SEM work was performed in the EPIC facility of NUANCE Center at Northwestern University. NUANCE Center is supported by the NSF-NSEC, NSF-MRSEC, Keck Foundation, the State of Illinois, and Northwestern University.

Powder X-ray Diffraction (PXRD). The samples were examined by X-ray powder diffraction for identification purposes and to assess phase purity. Powder patterns were obtained using a CPS 120 INEL X-ray powder diffractometer with Ni-filtered Cu Kα radiation operating at 40 kV and 20 mA and equipped with a position-sensitive detector. Samples were ground and spread on a glass slide. In order to avoid the rehydration of **MINOF-1'**, the sample for the PXRD measurement of this compound was prepared inside a dry glovebox. The sample was placed inside a sealed plastic bag and then transferred outside the box. The PXRD pattern of **MINOF-1'** was recorded immediately after the sample was removed from the sealed plastic bag. The purity of phases was confirmed by comparison of the X-ray powder diffraction patterns to ones calculated from single crystal data using the NIST Visualize 1.0.1.2 software.

X-ray Crystallography. A STOE imaging plate diffraction system (IPDS-2) using graphite-monochromatized Mo Kα radiation, was used for data collection. The data were collected at room temperature (for **MINOF-1**) or 200 ^{0}C (for **MINOF-1'**) over a full sphere of reciprocal space, up to 32-35° in θ. Cell refinement, data reduction and numerical absorption correction were carried out using X-area suite program. The intensities were extracted by the program XPREP(Sheldrick, G. M. In *SHELXTL*; 5.1 ed.; Bruker-AXS: Madison, WI, 1998). The structures were solved with direct methods using SHELXS and least square refinement were done against F_{obs}^2 using routines from SHELXTL software (Sheldrick, G. M. In *SHELXTL*; 5.1 ed.; Bruker-AXS: Madison, WI, 1998). In order to limit the disorder of the guest solvent molecules in **MINOF-1**, various restraints (ISOR, DELU, SIMU) have been applied in the refinement of the crystal structures. The low quality of the refinement for the structure of **MINOF-1'** is due to the poor diffraction of the crystal because of the partial loss of the crystallinity for the desolvated structure.
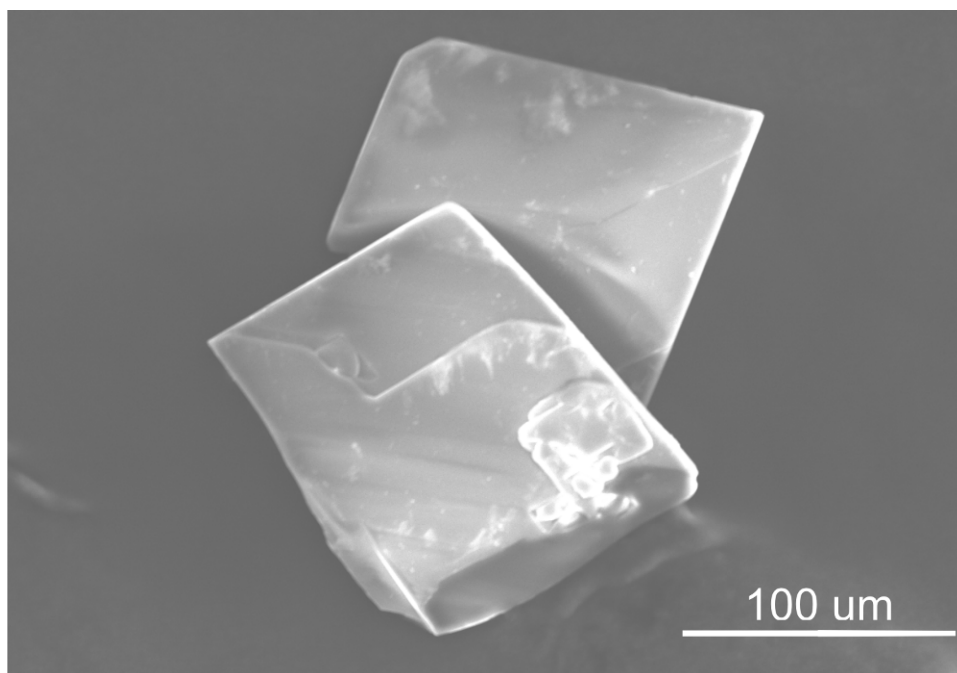
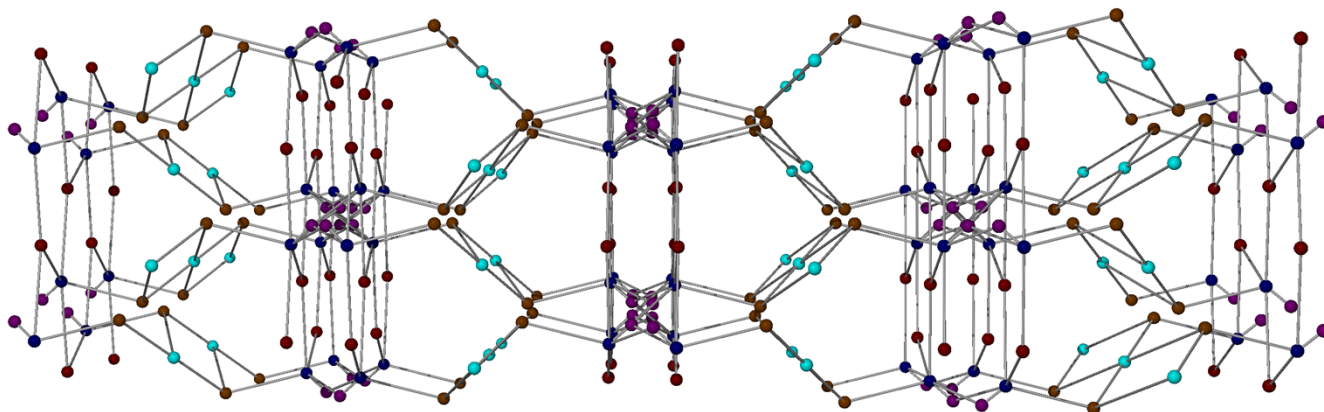Fig. S1. Scanning Electron Microscopy (SEM) image of plate-like crystals of **MINOF-1**.

Fig. S2. View of the unique 3,3,4,4,8-connected net of the **MINOF-1**. Cu_2(paddle-wheel SBUs), cyan; Cu_3 (Cu_2, Cu_3, Cu_4 subunit), blue; SeO_3^{2-}, purple; btc^{3-} type A, brown; btc^{3-} type B, red.
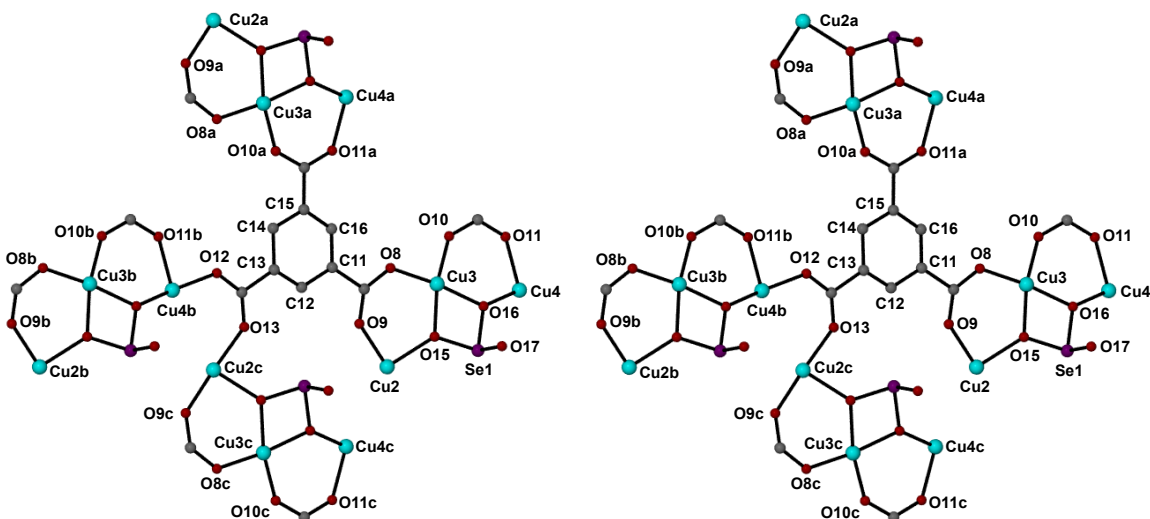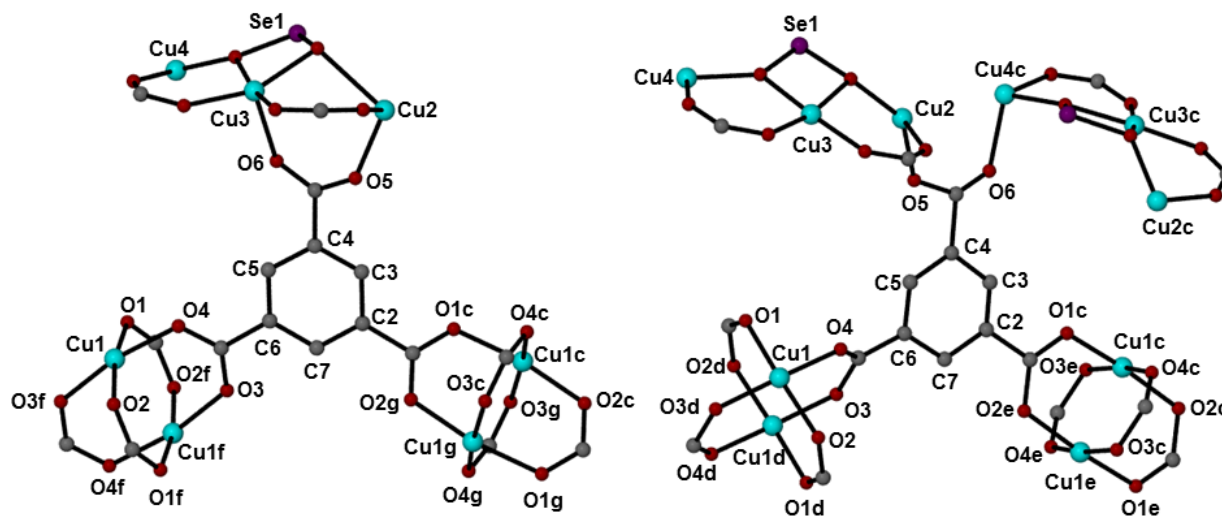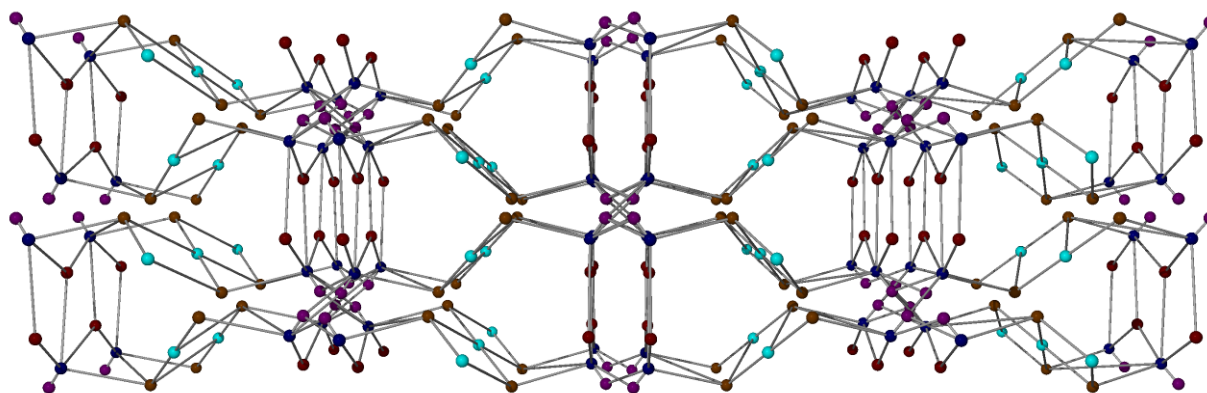
Fig. S3. The coordination environment around btc^{3-} type B in **MINOF-1** (left) and **MINOF-1'** (right). Symmetry codes: a: x, 1-y, z-1/2 ; b: x, y, z-1; c: x, -y, z-1/2.

Fig. S4. The coordination environment around btc^{3-} type A in **MINOF-1** (left) and **MINOF-1'** (right). Symmetry codes: c: x, -y, z-½; d: ½-x, ½-y, -z; e: ½-x, y-½, -z −½; f: 3/2-x, ½-y, 1-z; g: 3/2-x, y-½, ½-z.

Fig. S5. View of the unique 3,4,4,4,9-connected net of the **MINOF-1'**. Cu_2(paddle-wheel SBUs), cyan; Cu_3 (Cu_2, Cu_3, Cu_4 subunit), blue; SeO_3^{2-}, purple; btc^{3-} type A, brown; btc^{3-} type B, red.

Gas Sorption Measurements

Low-pressure nitrogen, hydrogen, carbon dioxide and methane adsorption measurements were carried out on an ASAP 2020 instrument from Micromeretics. Ultra-high purity grade N_2 (99.999%), He (99.999%), H_2 (99.999%), CO_2 (99.999%) and CH_4 (99.9995%) were used for all adsorption measurements. Prior to analysis, as-made **MINOF-1** crystals were transferred to a pre-weighted sample tube. The tube was then transferred to the outgassing station were the sample evacuated under vacuum at 200 ^0C for 20 h. After evacuation, the sample and tube were re-weighed to obtain the precise mass of the evacuated sample. Finally, the tube was transferred to the analysis port of the gas adsorption instrument.

Gas selectivity using the IAST approach

The single-component adsorption isotherms were analyzed by fitting the data with the following virial-type equation:

$$p = \frac{V}{K}\exp(c_1 v + c_2 v^2 + c_3 v^3 + c_4 v^4)$$

(1)

where, p is the pressure in Torr, v is the adsorbed amount in mmol g^{-1}, K is the Henry constant in mmol g^{-1} $Torr^{-1}$ and c_i are the constants of the virial equation.

The free energy of desorption at a given value of temperature and pressure of the gas is obtained from the analytical integration of eq. (1):

$$G(T,p) = RT\int_0^p \frac{n}{p}dp = RT(v + \frac{1}{2}c_1 v^2 + \frac{2}{3}c_2 v^3 + \frac{3}{4}c_3 v^4 + \frac{4}{5}c_4 v^5)$$

(2)

The free energy of desorption is a function of temperature and pressure, $G(T,p)$, and describes the minimum work (Gibbs free energy) that is required to completely degas the adsorbent surface. For a binary mixture of components, i and j, eq. (2) yields the individual pure loadings v_i^o, v_j^o at the same free energy of desorption:

$$G_i^0(v_i^0) = G_j^0(v_j^0)$$

(3)

The partial pressures of i and j components in an ideal adsorption mixture are given by:

$$py_i = p_i^0(v_i^0)x_i$$

(4)

$$py_j = p_j^0(v_j^0)x_j$$

(5)

where, y_i (=1-y_j) and xi (=1-x_j) is the molar fraction of component i in the gas phase and the adsorbed phase, respectively and p_i^o, p_j^o is the pure component pressure of i and j, respectively.

After solving equations (3)-(5) and equation (1), the selectivity for the adsorbates i and j ($s_{i,j}$) and the total pressure (p) of the gas mixture were obtained from eq. (6) and eq. (7), respectively.

$$s_{i,j} = \frac{x_i/y_i}{x_j/y_j} = \frac{p_j^0}{p_i^0}$$

(6)

$$p = \sum_i^j p_i^0 x_i$$

(7)

Isosteric heat of adsorption

The gas adsorption isotherms of **MINOF-1´** at different temperatures were described and analyzed using the following virial-type equation[1]:

$$\ln p = \ln v + \frac{1}{T}\sum_{i=0}^{m} a_i v^i + \sum_{i=0}^{n} b_i v^i \tag{8}$$

where, p is the pressure in Torr, v is the amount adsorbed in mmol g^{-1}, T the temperature in K and a_i, b_i are adjustable parameters. m, n represent the order of polynomials that are required to adequately describe the isotherms.

The loading dependent isosteric heat of adsorption, q_{st}, was calculated using the following expression:

$$q_{st} = -R\sum_{i=1} a_i v_i \tag{9}$$

where R is the universal gas constant.
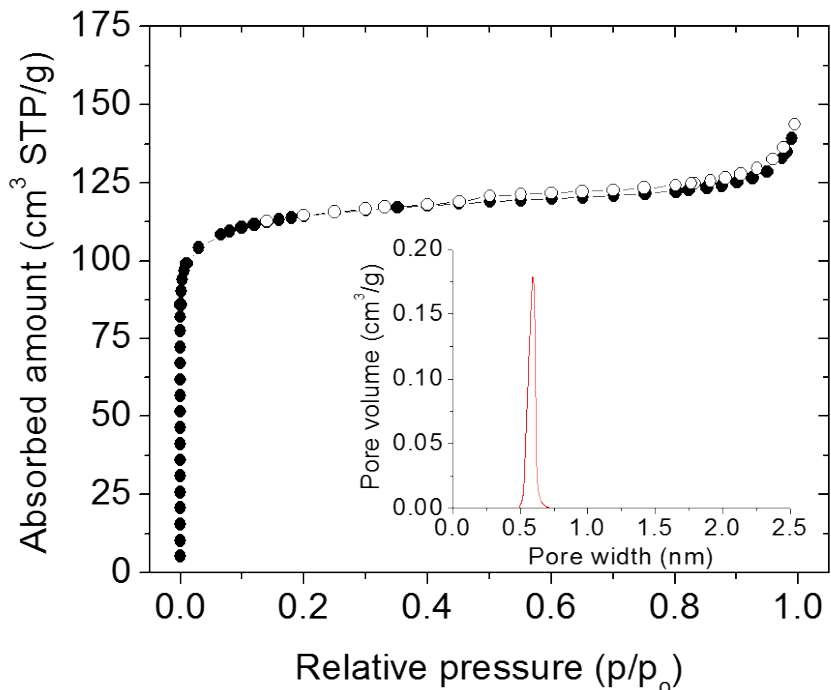
Fig. S6. Nitrogen adsorption (solid) and desorption (open circles) isotherms of microporous **MINOF-1´**. Inset: The NLDFT size-distribution of pores calculated from the adsorption branch.
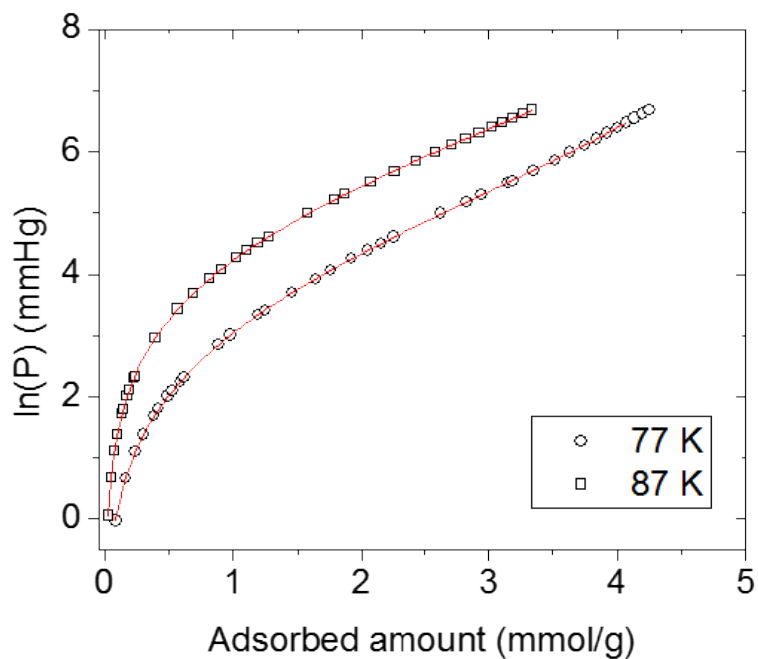
Fig. S7. Adsorption isotherms of hydrogen for microporous **MINOF-1´** material at 77 and 87 K. The corresponding red lines are fits to the data according to the appropriate virial-type equations.
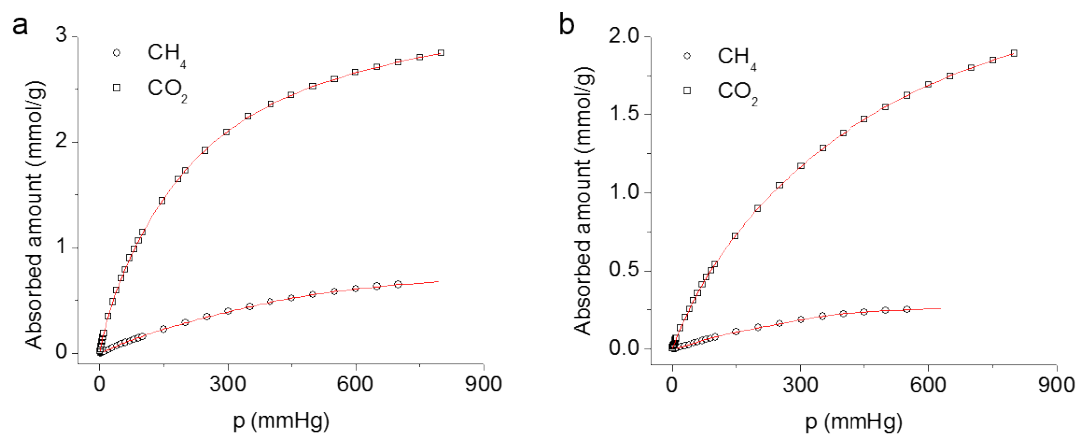

Fig. S8. Adsorption isotherms for CO_2 (squares) and CH_4 (circles) of microporous **MINOF-1´** at (a) 273 and (b) 298 K. The corresponding red lines are fit to the data using IAST model.
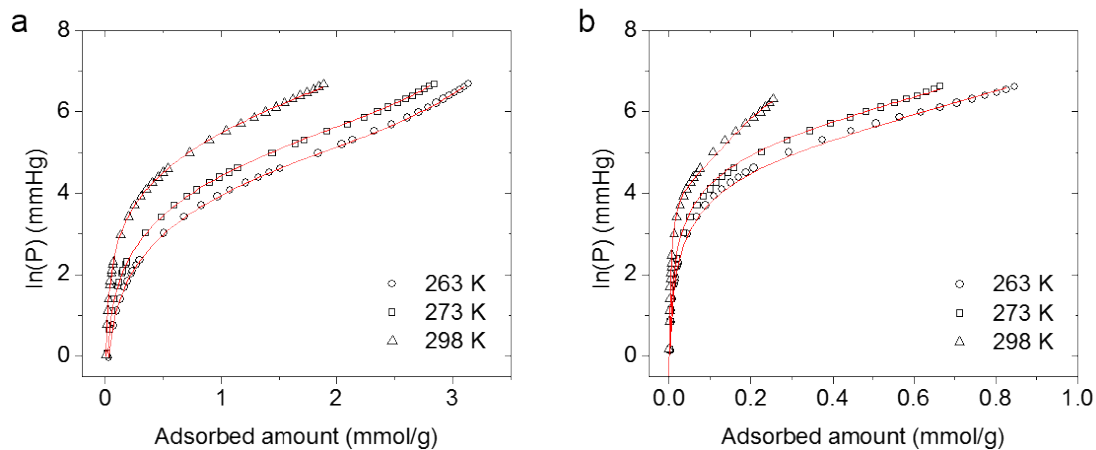
Fig. S9. Adsorption isotherms of carbon dioxide (a) and methane (b) for microporous **MINOF-1´** at 263, 273 and 298 K. The corresponding red lines are fits to the data according to the appropriate virial-type equations.

References

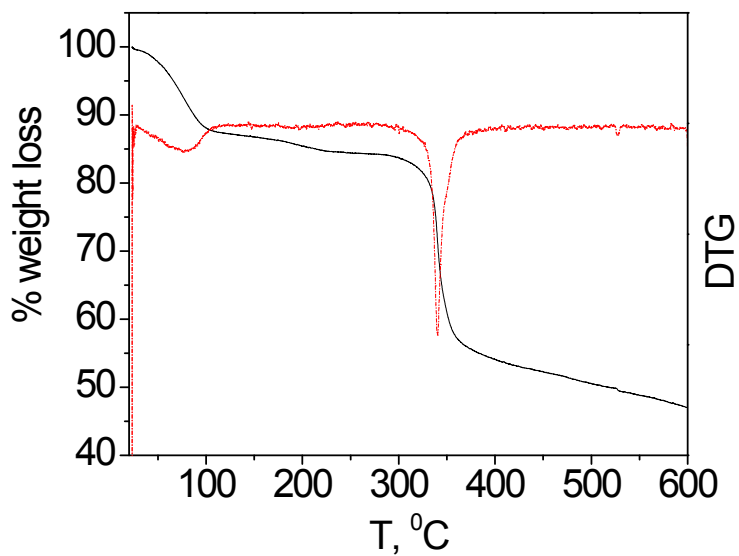1. L. Czepirski and J. Jagiello, *Chem. Eng. Sci.*, 1989, **44**, 797.

Fig. S10. The TG (red)/DTG (dashed line) curves for **MINOF-1.**

The initial losses (~15.6 %) occurring from 25-260 ˚C are due to the elimination of lattice and coordinating H_2O molecules (calculated weight loss for 2 coordinating and 6 lattice H_2O solvent molecules = 15.3%). The following weight losses are attributed to the decomposition of trimesate and selenite ligands.
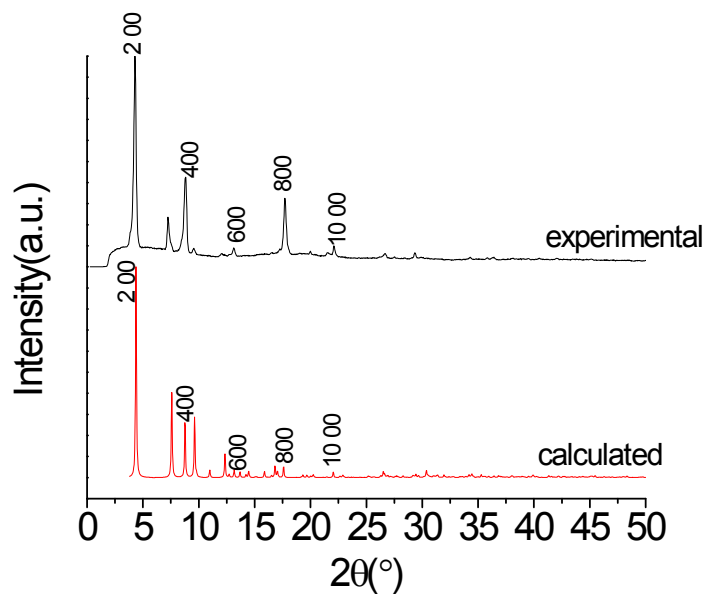

Fig. S11. Experimental and calculated PXRD patterns of **MINOF-1**. There is a strong preferential orientation effect due to the plate-like shape of the crystals of **MINOF-1** that leads to the significant increase of the intensities for (*h00*) peaks.
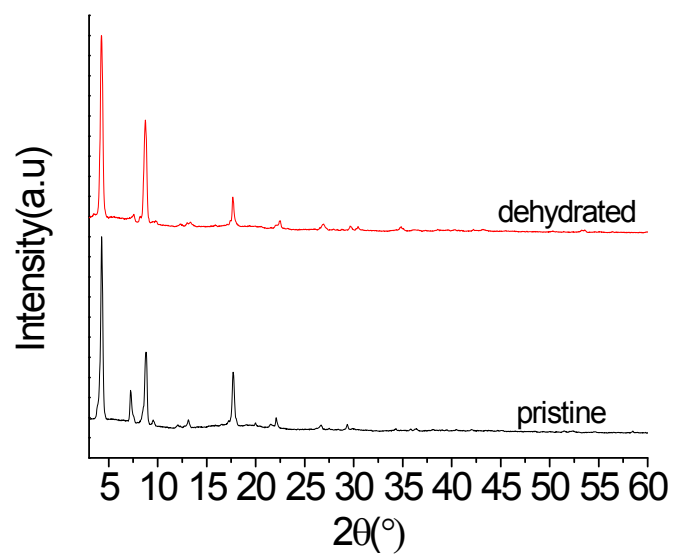
Fig. S12. PXRD patterns of pristine **MINOF-1** and dehydrated **MINOF-1'**.
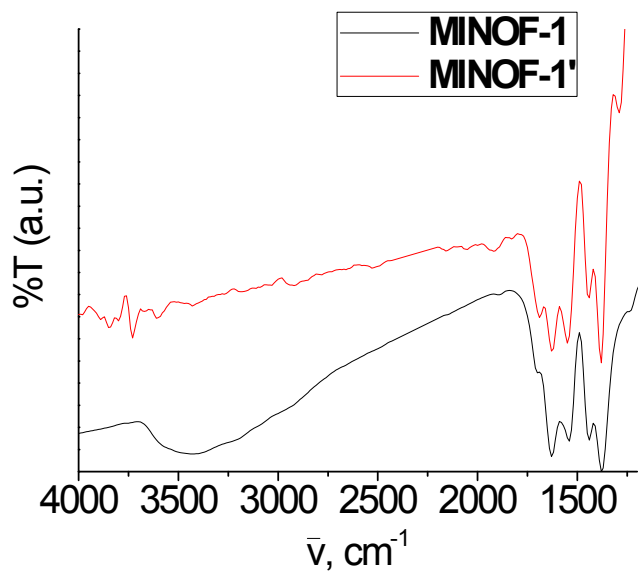

Fig. S13. Mid-IR spectra of pristine **MINOF-1** and dehydrated **MINOF-1'**.